Graphical abstract

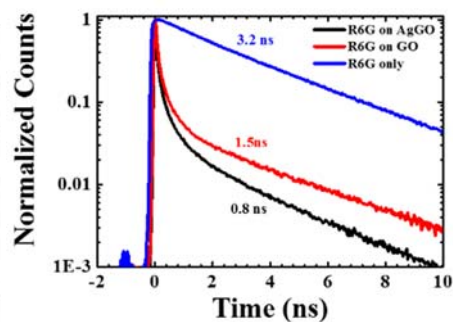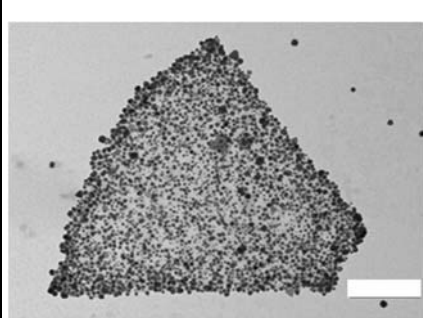|	
Influence of graphene oxide/Ag nanoparticle composites on the fluorescence properties of organic dyes John J. Gough, Katarzyna E. Siewerska, Sam Mehigan, Damien Hanlon, Claudia Backes, Zahra Gholamvand, Beata M. Szydłowska, Werner J. Blau, Eithne McCabe and A. Louise Bradley	Graphene oxide/Ag nanoparticle (AgGO) composite materials have been studied to examine the role of the individual components on the fluorescence quenching of three fluorescent dyes. Distinct differences in the way in which each dye is influenced by the individual components of the AgGO composite is observed and quantified using time-resolved photoluminescence.

Influence of graphene oxide/Ag nanoparticle composites on the fluorescence properties of organic dyes

John J. Gough[1,*], Katarzyna E. Siewerska[1], Sam Mehigan, Damien Hanlon, Claudia Backes, Zahra Gholamvand, Beata M. Szydłowska, Werner J. Blau, Eithne McCabe and A. Louise Bradley

School of Physics and CRANN, Trinity College, Dublin 2, Ireland

*Corresponding author; e-mail: goughj3@tcd.ie, phone: +353-868977625.
[1]These authors contributed equally to this work.

ABSTRACT

Graphene oxide/Ag nanoparticle (AgGO) composite materials have been proposed for surface enhanced Raman scattering (SERS) detection of fluorescent dye molecules. In this study we examine the role of the different components of the Ag nanoparticle (NP) decorated graphene oxide (GO) composite on the fluorescence quenching properties of three fluorescent dyes; Rhodamine 6G (R6G), Rhodamine B (RhB) and Sulforhodamine 101 (SR101), with emission spanning from approximately 550 nm to 750 nm. The influence of the dye emission properties, spectrum and quantum yield, on the SERS detection on GO and AgGO substrates has been characterized. The AgGO substrate yields large increases in the measured average Raman signal-to-noise ratios for all three dyes, with the greatest enhancements observed for R6G and SR101. Distinct differences in the way in which each dye is influenced by the individual components of the AgGO composite is observed using time-resolved photoluminescence. The fluorescence quenching efficiency on bare GO is largest for R6G, while the fluorescence lifetime of SR101 is most strongly influenced by the adsorption of the Ag NPs. The SERS enhancement on the AgGO composite benefits most from the fluorescence quenching for R6G, while the localized field enhancement due to the Ag NPs is a more significant factor in the increased Raman scattering signal for SR101.

Keywords: Fluorescence quenching; 2D materials; graphene; energy transfer; plasmonics, Raman scattering.

1. INTRODUCTION

Raman spectroscopy is a powerful technique that can be employed to study and characterize molecular structures in detail, but is limited by low sensitivity. Surface enhanced Raman scattering (SERS) can achieve large Raman scattering intensity enhancements allowing for highly sensitive detection of low concentrations of analytes. First discovered in the 1970s the enhancement is attributed to two mechanisms, chemical enhancement and local electromagnetic field enhancement.[1-3] Large localized electromagnetic fields can be experienced by analytes located close to the surface of a metal, particularly nanostructured or roughened surfaces. Enhancement of SERS by nanostructured metals has been an intense area of research over the past number of years as reviewed in the literature.[4-6] Materials commonly used for SERS studies are those of noble metal NPs, such as Au or Ag, due to the relatively straight forward synthesis which provides control over size and shape of the NPs.[7-10] These noble metal NPs can also give rise to metal/surface enhanced fluorescence.[11-13] This fluorescence enhancement can prove detrimental to SERS measurements as the fluorescence masks the Raman scattering peaks.

More recently, graphene and its derivatives, graphene oxide (GO) and reduced-graphene oxide (rGO), have been investigated as SERS substrates and have been shown to produce strong chemical enhancement, which is attributed to charge transfer from the graphene substrate.[14-16] The atomically flat graphene substrate provides the conditions for sufficiently close proximity of the analytes to the substrate to achieve efficient charge transfer. Enhancements as large as 10^3 have been reported for rGO.[17] Graphene and its related-materials have also been shown to demonstrate large fluorescence quenching efficiencies over significant distances.[18-24] The quenching of fluorescence occurs due to non-radiative energy transfer such as Förster resonance energy transfer or charge transfer. Förster resonance energy transfer is seen to dominate for separations of > 4 nm as the charge transfer efficiency is more strongly distance dependent.[19, 21, 22, 25]

There are two specific forms of Raman scattering in terms of excitation, namely non-resonant and resonant Raman scattering. For non-resonant Raman scattering the excitation wavelength is of lower

energy than the analyte's electronic absorption band, while in the case of resonant Raman scattering the excitation wavelength overlaps spectrally with the analyte's electronic absorption band. Resonant excitation can enhance the Raman scattering signal by several orders of magnitude,[26] however, it can be masked by the fluorescence background arising as a result of the resonant excitation. Therefore, the fluorescence quenching properties of graphene-related substrates can also lead to improvements in the detection of Raman scattering signals from fluorescent molecules.[27]

The possibility to combine the quenching properties of graphene-based materials with the advantages of nanostructured metals could allow for a robust multipurpose SERS substrate. To this end, AgGO composites, in particular, have received much attention.[28-33] The graphene-based substrates for SERS can be produced using cost effective, solution based processing of GO and rGO from graphite powder.[28-32, 34-47] Such processing allows for scalable production and offers large area coverage compared to graphene which is generally produced in minute quantities through mechanical and chemical exfoliation[34, 35] or epitaxial based growth methods.[34, 35, 48] Recent reports have demonstrated that the reduction of metallic salts on GO/rGO results in GO sheets decorated with metallic NPs.[28, 30, 37, 38, 40, 42] This decoration of GO with NPs can also be achieved via alternative methods such as electrostatic attraction,[29] liquid-liquid interface methods[36] and 2-step chronoamperometry deposition[46] among others.[31, 32, 39, 41, 43-45, 47] The adsorption of densely packed plasmonic metallic NPs onto the GO substrate allows for the formation of 'hot-spots'; the regions of high local electromagnetic field which enhance the intensity of the Raman scattering signal. There have been multiple reports on metal NP decorated graphene derived SERS substrates for fluorescent analytes which describe many novel fabrication techniques using nanoparticles of different geometries, concentrations and metals.[28, 29, 33, 36-47, 49-52] While these studies report improved SERS sensitivity, there has been no direct study of the interplay between SERS and fluorescence on the same substrate. A combined study of Raman scattering and fluorescence can probe the influence of the dye quantum yield, any impact of metal enhanced fluorescence due to the Ag NPs and whether there is a spectral dependence.

In this study we investigate the effect of the AgGO composite on the emission properties, as well as the Raman scattering signals, of three organic dyes, Rhodamine 6G (R6G), Rhodamine B (RhB) and

Sulforhodamine 101 (SR101), with emission spanning from approximately 550 nm to 700 nm. The AgGO composite can support a number of competing processes: enhanced Raman signals due to the Ag NPs and/or GO flakes, enhanced or quenched fluorescence due to the Ag NPs depending on the properties of the localized surface plasmon, as well as fluorescence quenching by the GO flakes. By studying the emission and Raman spectroscopy it is possible to examine the contributions of various processes to the enhanced SERS signals for each of the dyes. We present complementary studies of the impact of the various constituents of the composite substrate on the emission and Raman spectra. The emission properties were characterized using spectral and time-resolved photoluminescence (PL) measurements. While the GO substrate more efficiently quenches the dye fluorescence, the time-resolved photoluminescence (TRPL) data shows that the dye molecules are more strongly coupled to the AgGO composite. Higher levels of dye fluorescence are observed on the AgGO composites than on bare GO substrates and the Raman signals are also significantly enhanced. A concentration dependent study reveals the SERS signal detection limits for each dye on the AgGO substrate. The improvement in the SERS signal is quantified by a signal-to-noise ratio (*SNR*). The AgGO composite shows improved performance for all three dyes, and strong correlation between the TRPL data and the Raman scattering results is observed.

2. EXPERIMENTAL DETAILS

2.1 Materials

Expandable graphite flakes (1721, Asbury Graphite Mills, US) with flake size average > 500 μm were used as starting material for GO synthesis. Chemicals used for GO synthesis included potassium permanganate ($KMnO_4$), sulphuric acid (H_2SO_4 97%), hydrochloric acid (HCl 37%) and hydrogen peroxide (H_2O_2 30%). Chemicals used for the AgGO synthesis were Poly-(N-vinyl-2-pyrrolidone) (PVP) (Mw 40,000) and silver nitrate ($AgNO_3$) (Mw 169.87). The fluorescent dyes used in the experiments were Rhodamine 6G (R6G), Rhodamine B (RhB) and Sulforhodamine 101 (SR101).

Unless otherwise stated all chemicals and dyes were purchased from Sigma Aldrich. The dyes were obtained in powder form and dissolved in Millipore water.

2.2 Synthesis of GO

Large GO sheets were prepared by modified Hummers'[53] method using expandable flake graphite with a size of 500 - 600 μm as raw material. In a typical procedure, graphite flakes were heated in a 100 W microwave for 15 s to produce expanded graphite (EG) (volume expansion ratio 70 times) as the precursor for GO synthesis. Then 4 g of EG and 500 ml of H_2SO_4 were mixed and stirred in a three neck flask for 2 hrs. Next, 20 g of $KMnO_4$ was gradually added to the mixture. After 24 hrs of stirring at room temperature, the mixture was then transferred into an ice bath and 500 ml of deionized water and 100 ml of H_2O_2 were added dropwise into the mixture under controlled temperature (T < 60 °C) resulting in a colour change from dark green to golden yellow. Having stirred for another 30 mins, the resulting oxidized EG particles were washed and centrifuged with HCl solution (9:1 vol water: HCl) three times, then centrifuged again and washed with deionized water. Repeated centrifugation and washing steps with deionized water were carried out until a neutral solution (pH ≥ 5) was achieved. During the washing process, oxidized EG particles were exfoliated to GO sheets resulting in a highly viscous honey like solution with concentrations above 4.5 mg/ml.

2.3 Synthesis of AgGO

The obtained solution of GO in water was then further sonicated for 1 hour and a stock solution of 1.6 mg/ml was prepared for use as the precursor for the synthesis of the AgGO composite. The AgGO composite was prepared according to the method described by Zhang *et al.*[28] With this synthesis, 1.88 g PVP was dissolved in 8 mL of GO solution. The solution was then heated to 60 °C under constant stirring. Once the GO solution had reached 60 °C, 3 mL of 188 mM $AgNO_3$ in water was added and stirred for a further 5 minutes. The stirring was then stopped and the reaction was allowed to proceed for 24 hrs. To obtain complete Ag NP coverage of the GO flakes the concentration of GO in the reaction solution was reduced to 0.01 mg/mL. The product of the reaction was then centrifuged at 9000 RPM/5705 g using a Labnet Spectrafuge 7M (6.3 cm centrifuge radius and a 12 x 1.5 mL rotor) for 20

minutes and washed with Millipore water. This step was repeated 5 times to remove all excess unbound Ag NPs. The resulting AgGO was then re-dispersed in 5 mL Millipore water and sonicated in a Bandelin Sonorex RK31 ultrasonic bath with a frequency of 35 kHz and peak output power of 160 W for 30 minutes.

2.4 Microscopy

Scanning electron microscope (SEM) images were recorded using a Carl Zeiss Ultra SEM. 10 µL of the dispersion was dropcast onto a Si/SiO_2 wafer with a 300 nm oxide layer and allowed to dry in a fume hood. Transmission electron microscope (TEM) images were recorded using a JOEL 2100 TEM operated at 200 kV. Atomic force microscope (AFM) was carried out using a VeecoNanoscope-IIIa (Digital Instruments) system equipped with an E-head (13 µm scanner) in tapping mode. A 10 µL drop of the dispersion was deposited on a pre-heated (180 °C) Si/SiO_2 wafer with an oxide layer of 300 nm. After deposition, the wafer was rinsed with ~5 mL of deionized water. Typical image sizes ranged from 6 x 6 μm^2 to maximum 10 x 10 μm^2. As the nanosheets were large, scan rates of 0.5-0.8 Hz were applied with 512 lines per image.

2.5 Optical Measurements

Extinction, scattering and absorption measurements were performed using a Perkin-Elmer Lambda 650 S UV-Vis spectrometer equipped with a 150 mm integrating sphere. 50 µL of each stock solution was dispersed in 3 mL Millipore water for these measurements. To distinguish between contributions from absorption and scattering to the extinction spectra, the dispersions were measured in the integrating sphere using a custom-built sample holder to place the cuvette in the centre of the integrating sphere. It should be noted that the cuvettes need to be transparent on all sides. The absorption spectrum is obtained from the measurement inside the sphere. While the extinction measurement is obtained from a measurement outside the sphere. This allows the scattering spectrum to be calculated as extinction-absorption.

Adsorption capacity measurements were performed to measure the percentage of each dye adsorbed on the AgGO composite. For these measurements, dye solutions were prepared to a concentration of 4 x

10^{-7} M, to replicate the conditions in the TRPL measurements. To prepare the dye + AgGO solutions, 50 µL of stock AgGO solution was added to 2 mL of 4×10^{-7} M dye solution. The solution was mixed and sonicated for 20 seconds, then allowed to incubate for 3 hours at room temperature. The solutions were then centrifuged at 9000 RPM/5705 g for 20 minutes to precipitate the AgGO and consequently the dye adsorbed on the AgGO from the solution. Absorption measurements were then performed on the supernatant. To prepare the dye only reference samples, 50 µL of Millipore water was added to 2 mL of 4×10^{-7} M dye solution.   These measurements were carried out using a Cary 50 UV-Vis spectrometer using 1 cm path length cuvettes.

PL measurements were performed using an Andor Shamrock sr-303i spectrometer with an Andor Newton 970 EM-CCD under 90 ps pulsed excitation from a 405 nm laser with a repetition rate of 10 MHz and an integration time of 4 ms per pixel. The PL was collected using a 40× microscope objective (NA = 0.65). The PL measurements were recorded over areas of 5 µm x 5 µm. The laser spot size was ~ 500 nm. For R6G and RhB, the excitation powers were 4.2 µW and 6.3 µW, respectively. In the case of SR101, the excitation power was 8.4 µW and electron multiplication (EM) was doubled to compensate for the low absorption of the dye at the excitation wavelength.

TRPL measurements were performed using a PicoQuant Microtime200 time-resolved confocal microscope system using an excitation of 90 ps pulses at a wavelength of 405 nm with a repetition rate of 10 MHz and an integration time of 4 ms per pixel. The emission was collected using a 40× microscope objective (NA = 0.65). The TRPL measurements were recorded over areas of 5 µm x 5 µm. The PL and TRPL measurements for each dye and dye-substrate combination were recorded at the same positions. The laser spot size was ~ 500 nm. The excitation powers were 0.11, 0.21 and 0.42 µW for R6G, RhB and SR101, respectively, taking account of the spectral mismatch between the excitation wavelength and the absorption bands of the individual dyes. For the PL and TRPL measurements, 50 µL of 1×10^{-6} M dye solution was added to 25 µL Millipore water and 50 µL of AgGO/GO, giving a dye concentration of 4×10^{-7} M. For the dye only measurements 50 µL of 1×10^{-6} M dye solution was dispersed in 75 µL Millipore water. The solutions were sonicated for ~ 60 s and spincast onto a hydrophilic quartz substrate at 2000 RPM for 180 s.

Raman measurements were performed using a Horiba Jobin Yvon LabRAM HR800 Spectrometer in air under ambient conditions. The Raman emission was collected by a 100× objective lens (N.A. = 0.8, spot size ~1 µm) and dispersed by 600 gr/mm. Prior to the acquisition of the samples, the spectral position was calibrated to the 521 cm^{-1} peak of Si/SiO$_2$. The samples used for the Raman study were prepared from a stock dye solution of 10^{-3} M and dilute AgGO solution in a 1:1 ratio. The mixture was left to settle for several hours and subsequently sonicated for 1 minute to disperse the AgGO flakes in the solution. Next 10 µL of the mixture was dropcast onto a glass cover slide and left to air dry in a fume hood. This technique ensures sufficient adsorption of dye molecules onto the substrate. Based on the absorption bands of the fluorescent dyes, the 532 nm excitation wavelength was chosen. Samples with R6G and RhB were excited with a laser power of 1.94 µW and samples with SR101 were excited with a laser power of 15.1 µW. The accumulation time was ~ 6 seconds. For the *SNR* and apparent enhancement factor (*AEF*) calculations, the background was subtracted from the Raman spectra. For evaluation of the *AEF*, comparative spectra were taken from samples prepared from 10 µL of 10^{-3} M dye solution.

3. RESULTS AND DISCUSSION

Following the synthesis of the AgGO composite, the Ag NP coverage on the GO flakes was investigated using TEM, SEM and AFM. The high density coverage of the GO flakes with Ag NPs can be seen in the TEM and SEM images in Fig. 1(a) and (b), respectively. The TEM images revealed that there is a range of Ag NP sizes and morphologies on the AgGO composite. Multiple TEM images of AgGO flakes were taken and the diameters of 340 Ag NPs were measured to determine the average Ag NP diameter, see Fig. 1(d). The Ag NP mean diameter the AgGO composite was found to be (40 ± 16) nm. SEM images were recorded to gain a better visual of the surface morphology of the individual AgGO flakes. The SEM image in Fig. 1(b) clearly demonstrates the complete and high density coverage of Ag NPs on the GO flake. AFM measurements of the AgGO flakes were also recorded to ensure that the GO was coated with Ag NPs on both sides of the flake. A typical AFM image of an AgGO flake can be seen in Fig. 1(c). The AFM measurements gave the height of the AgGO composite flakes in the range

50 – 100 nm, verifying the presence of Ag NPs on both sides of the GO flakes. XRD measurements (not shown) were performed on the bare GO flakes and show a sharp diffraction peak at 10.03° corresponding to the reflection from the (001) plane and inter-planar spacing of 0.88 nm,[54] thus confirming that the bare flakes are GO.

UV-Vis extinction spectroscopy was performed to identify the spectral characteristics of the AgGO composite. The extinction spectra of the GO, Ag NPs and AgGO composite in aqueous solution are shown in Fig. 2(a). The typical extinction spectrum associated with the localized surface plasmon resonance of Ag NPs is clearly seen in Fig. 2(a). The extinction spectrum of the AgGO is significantly broader and shows a red-shift in the peak extinction wavelength as compared to the Ag NPs alone. The red-shift of the peak and broadening of the extinction spectrum is attributed to increasing Ag NP size and polydisperse distributions in combination with the increased interaction between the Ag NPs due to the dense packing of the Ag NPs on the GO flake. This interaction results in a more prominent role of scattering at the longer wavelengths in the extinction spectrum.[55]

To confirm the role of scattering from the Ag NPs on the AgGO composite, UV-Vis measurements were performed using an integrating sphere to separate the extinction spectrum into the absorption and scattering components. The extinction cross section, σ_{Ext}, is given by:

$$\sigma_{Ext} = \sigma_{Abs} + \sigma_{Sca} \qquad (1)$$

where σ_{Abs} and σ_{Sca} are the absorption and scattering cross sections, respectively.[56] The extinction, absorption and scattering spectra of AgGO composite are shown in Fig. 2(b), where it can be seen that the scattering plays a more dominant role than absorption in the overall extinction spectrum, particularly at longer wavelengths. The Raman excitation wavelength, 532 nm, overlaps the localized surface plasmon resonance extinction spectrum and therefore, it is expected that there will be local field enhancement at this wavelength which is beneficial for SERS. The extinction spectrum for each dye in aqueous solution is shown in Fig. 3(a). The vertical black dash line indicates the Raman excitation wavelength, 532 nm. However, as can be seen in Fig. 3(b) the peak emission wavelengths of R6G, RhB and SR101 are also located close to the maximum of the scattering spectrum which can lead to metal enhanced fluorescence.[11-13] This can be deleterious for SERS as the emission can mask the Raman

spectra, reducing the detection sensitivity. Fig. 3(c) shows the percentage of dye adsorbed on the AgGO substrates, this represents the adsorption capacity of the AgGO substrate for each dye. It is clear from Fig. 3(c) that both R6G and RhB display similar levels of adsorption to the AgGO. For SR101, approximately half the number of molecules have adsorbed to the AgGO compared to R6G and RhB.

TRPL measurements were carried out to investigate the effect of the GO and AgGO composite flakes on the fluorescence properties of the three organic dyes. As discussed earlier, it is known that GO is a strong fluorescence quencher,[19] however the quenching properties of the AgGO composite are less studied. As mentioned above, there are approximately twice as many R6G and RhB molecules adsorbed on the AgGO substrates than SR101 molecules, however, this will not affect the TRPL results as the lifetime measurements are concentration independent at the concentrations used for both the TRPL and PL measurements.[57] Fig. 4 shows the fluorescence decays for the three dyes; (a) R6G, (b) RhB and (c) SR101. The fitting of the dye only decay curves was carried out using a single exponential decay curve, given by

$$I(t) = I_1 e^{-\frac{t}{\tau_1}} \tag{2}$$

where I_1 is the intensity amplitude for the single decay having a lifetime of τ_1. The fitting of the decay curves for the dye on the GO and AgGO substrates were performed using a bi-exponential decay curve due to the introduction of an additional dye decay pathway when coupled to the substrates. The fitting of the bi-exponential decay curve is given by

$$I(t) = I_1 e^{-\frac{t}{\tau_1}} + I_2 e^{-\frac{t}{\tau_2}} \tag{3}$$

where I_1 and I_2 are the intensity amplitudes for both decays having lifetimes of τ_1 and τ_2, respectively. The intensity weighted average lifetime, τ_{Avg}, is calculated from the fitting parameters as follows

$$\tau_{Avg} = \frac{I_1 \tau_1^2 + I_2 \tau_2^2}{I_1 \tau_1 + I_2 \tau_2} \tag{4}$$

All lifetime values for dyes on the GO and AgGO mentioned here are those of the average lifetime, τ_{Avg}. In all three cases, the TRPL shows a clear reduction in the fluorescence lifetime for the dyes adsorbed on GO compared to the dye alone, with a further reduction in the lifetime when the dye is adsorbed on the AgGO composite. This further reduction of the dye's fluorescence lifetime when on the AgGO

composite is attributed to processes associated with Ag NPs which can include an enhanced excitation rate, enhanced radiative rate and non-radiative energy transfer from the dye to the Ag NPs which can result in emission quenching via Joules heating or scattered radiation from the Ag NPs. These processes have been extensively reported in the literature.[58-61] The fluorescence lifetime values extracted from the decays can be used to obtain a direct measure of the quenching efficiency in the case of GO or the strength of interaction between the dye and substrate in the case of the AgGO samples which can be considered as a coupling efficiency. The efficiency, η, can be quantified by

$$\eta = 1 - {\tau_{DS}}/{\tau_D} \tag{5}$$

where τ_D is the fluorescence lifetime of the dye alone and τ_{DS} is the lifetime of the dye in the presence of the GO or AgGO composite substrate. The efficiencies for each dye on the GO and AgGO composite substrates can be seen in table 1, along with the quantum yields for each dye in aqueous solution.

Table 1: Efficiencies for dyes in the presence of GO and AgGO.

Fluorescent Dye	Quantum Yield	Efficiency, η	
		GO	AgGO
R6G	95 ± 14 %	53 ± 7 %	75 ± 10 %
RhB	43 ± 6 %	45 ± 8 %	66 ± 7 %
SR101	19 ± 3 %	21 ± 2 %	74 ± 8 %

The data in table 1 shows that the AgGO composite has a larger influence on the dye emission than the GO alone for all three dyes. R6G and SR101 show similar efficiency values on the AgGO composite with a reduction in the case of RhB. This indicates that the strength of interaction between RhB and the AgGO composite is less strong than for the other two dyes. It is noted that the quenching efficiency for SR101 on the GO flake is much lower than for R6G and RhB. The quenching efficiency due to nonradiative energy transfer can be strongly influenced by the spectral overlap between the dye and the GO as well as the dye quantum yield, both of which are lower for SR101. The efficiency of SR101 is recovered on the AgGO substrate which is attributed to the enhanced excitation and radiative rates due

to the presence of the Ag NPs as well as non-radiative energy transfer to the Ag NPs, as previously discussed.

The PL spectra for each dye on GO flakes and AgGO composites are shown in Fig. 4(d-f). The PL measurements reveal that in each case the emission intensity from the dyes is most strongly quenched when the dye is adsorbed on GO. When adsorbed onto the AgGO composite each dye shows an increase in the emission intensity relative to the GO substrate. This increase in emission intensity can be attributed to metal enhanced fluorescence due to the presence of Ag NPs on the AgGO substrate or an increase in the adsorption of the dye.[40]

To assess the advantage of the AgGO composite as a substrate for SERS when fluorescence is also excited we have chosen three dyes that can be excited by the same wavelength, 532 nm, with emission spanning the spectrum from 550 nm to 700 nm. In particular, the influence of the modified emission properties on the SERS detection is investigated. Raman spectroscopy using GO flake substrates and Ag NPs has also been carried out to probe how the different individual components of the AgGO composite influence Raman scattering signals. The Ag NP substrate used for the Raman measurements consists of unbound Ag NPs from the AgGO reaction solution, so that they are identical to those forming the AgGO composite. These Ag NPs were found to form clusters upon drying creating conditions for 'hot-spots', similar to the closely packed NPs on the AgGO composite. Fig. 5(a-c) shows Raman scattering spectra for each dye with a concentration of 10^{-4} M recorded on GO flake, AgGO composite and Ag NP substrates. The single spectra show qualitatively the influence of the AgGO composite and its components on the Raman scattering spectra. Quantitative analysis needs to take consideration of inhomogeneity across the substrate, and such an analysis, averaged over many measurements, is discussed in more detail below. The spectra on monolayer GO show a low background fluorescence consistent with the large fluorescence quenching efficiencies observed earlier. However, the Raman spectra peaks are barely visible. A large fluorescence background dominates the spectra on the Ag NP substrate for all dyes, with only some low intensity Raman peaks visible. For all dyes the Raman peaks are most intense on the AgGO substrate. The fluorescence background is flatter and quenched relative to the Ag NP samples. This reduction in the fluorescence background is attributed to the presence of GO in the AgGO composite material. The background signal level is found to be higher than for the

14

GO substrates, consistent with the increase in PL observed earlier. Despite the higher fluorescence for the AgGO composite the Raman peaks are clearly more visible. These results qualitatively demonstrate the enhancement of the Raman spectra peaks and fluorescence quenching in the presence of the AgGO composite.

To quantify the performance of the AgGO substrate over that of the Ag NPs alone, the signal-to-noise ratio (*SNR*) is considered, which is a measure of the detection sensitivity. The *SNR* measures the visibility of the Raman peaks over the background noise and is calculated according to equation (6).

$$SNR = \frac{S - N}{\sqrt{N}} \tag{6}$$

where *S* is the signal intensity and *N* is the noise intensity. Before calculating the *SNR*, the background was fitted and subtracted from the raw data. As the above formula shows large variations at low values of the noise intensity, the spectral position and noise value were carefully chosen to minimize uncertainty. The average background subtracted Raman spectra from 51 measurements using 10^{-4} M of each dye on Ag NP and AgGO substrates can be seen in Fig. 5(d-f). No changes in the peak positions were observed for the different substrates.

The Raman peak [noise] positions chosen to calculate the *SNR* for R6G, RhB and SR101 were 1362 cm^{-1}, 1511 cm^{-1} and 1508 cm^{-1} [1334 cm^{-1}, 1545 cm^{-1} and 1532 cm^{-1}], respectively. The results, presented in Fig. 6, show that the average *SNR* values are higher on the AgGO composite than on Ag NPs for each dye. This is attributed to larger enhancement of the Raman signal arising from the higher packing density of the Ag NPs on the GO flake, which acts as a scaffold for the Ag NPs, and to the quenching of the fluorescence of the dyes due to the presence of the GO substrate. In the case of R6G, there is a greater improvement in the average *SNR* value compared with RhB and SR101. This is in agreement with the spectra shown in Fig. 5. R6G fluoresces more strongly than the other two dyes; it has the highest quantum yield of the three dyes and the best overlap of the excitation wavelength at 532 nm with the absorption spectrum. Therefore, the impact of fluorescence quenching would be expected to show the greatest improvement in the *SNR* for this dye.

In order to identify the detection limit of the AgGO composite substrate, a concentration dependent study was carried out, the results of which are presented in Fig. 7. The spectra for concentrations above

10^{-7} M were easily obtained and hence it was possible to take an average over many spectra. The spectra shown in Fig. 7 are averaged over 30 spectra for dye concentrations of 10^{-3}, 10^{-5} and 10^{-6} M whereas 51 spectra were averaged for dye concentrations of 10^{-4} M. At lower concentrations (10^{-7}-10^{-9} M), the spectra were recorded at 'hot-spots' on the AgGO composite and a single spectrum showing the highest intensity Raman peaks observed is presented.

At the lowest concentrations the broad D and G Raman peaks from the GO in the AgGO composite are clearly visible in the 1300 cm^{-1} to 1700 cm^{-1} range. The detection limits for R6G, RhB and SR101 were found to be 10^{-9} M, 10^{-8} M and 10^{-8} M, respectively. These detection limits compare well with other reports in the literature. R6G is perhaps the most commonly studied SERS analyte. The detection limit of 10^{-9} M reported here is similar to that reported in reference 36 and lower than other reports on similar substrates.[38, 40] There are fewer SERS reports for RhB with similar substrates, though again the detection limit of 10^{-8} M for RhB is within the range of 10^{-7} M on a variety of treated graphene based materials[49] and 10^{-9} M on a composite material of Ag dendrites and rGO.[52] As far as the authors are aware these are the first reports for SR101 on an AgGO composite substrate.

From Fig. 7 it is clear that the quality of the spectra for each dye above the detection limit is excellent. All peaks are present and easily identifiable. The intensity of the Raman peaks was observed to increase with increasing dye concentration, except for the highest concentration of 10^{-3} M. This is reflected in the larger *SNR* at higher concentrations, shown in table 2. At the highest concentration (10^{-3} M) , the dye molecules are so densely packed that the overall spectral intensity is reduced due to self-absorption.[62, 63]

These spectra were used to calculate the *SNR* values, presented in table 2. The *SNR* quantifies the sensitivity of the AgGO composite substrate and can be used to assess the effectiveness of the AgGO composite as a viable SERS substrate for fluorescent dye analytes. To further analyse the impact of the AgGO composite on detecting a Raman scattering signal for a solution of a given concentration, we define an apparent enhancement factor (*AEF*)

$$AEF = \frac{I_{SERS}}{I_{glass}} \cdot \frac{C_{glass}}{C_{SERS}} \qquad (7)$$

where I_{SERS} is the intensity of the Raman peak, C_{SERS} is the dye concentration of the solution used to prepare the dye-AgGO sample, I_{Glass} is the intensity of the Raman peak in the spectrum from a dried sample prepared from dye solution with $C_{Glass} = 10^{-3}$ M drop cast onto a glass substrate. As mentioned earlier single measurements may or may not be recorded at a 'hot-spot', and each 'hot-spot' does not necessarily produce the same enhancement of the Raman scattering signal. The *AEF* is calculated using averaged spectra, as shown in Fig. 7. The Raman scattering spectra were recorded over multiple flakes to obtain an average spectrum for each dye concentration down to 10^{-6} M. This average peak intensity I_{SERS} at this lowest concentration is taken for the calculation of the *AEF*, where the peaks used are the same as for the *SNR* calculations. The *AEF* calculated for this solution concentration are 1×10^4, 2×10^3 and 6×10^4 for R6G, RhB and SR101, respectively. It is emphasized that these values represent an average not just the enhancement at a single 'hot-spot'. However, it is difficult to use previously published data as a comparison as there is no standardized method for calculating the *SNR* and *AEF* in terms of the specific Raman peaks used in the calculation. Consequently, these quantities will vary from study to study based on the choice of peak position and noise values, however they are valuable for comparing the impact of the AgGO composite across the three dyes.

Table 2. *SNR* for R6G (1362 cm^{-1}), RhB (1511 cm^{-1}) and SR101 (1508 cm^{-1}).

Dye Concentration	*SNR*			
	R6G	RhB	SR101	
10^{-9} M	7	-	-	
10^{-8} M	34	7	8	Single Hot-spots
10^{-7} M	64	27	58	
10^{-6} M	212	68	97	
10^{-5} M	277	101	138	Substrate Average
10^{-4} M	228	110	130	
10^{-3} M	132	57	59	

As previously described, AgGO composite for SERS benefit from the combination of enhancement of the Raman scattering signals and quenching of the background fluorescence. Comparison of the TRPL data and Raman data provides insight into the influence of each of these mechanisms for each dye. The *SNR* values presented in table 2 show a similar trend to the efficiency calculated from the TRPL data on the AgGO composite given in table 1. As discussed earlier this efficiency can be considered as a measure of the strength of interaction between the AgGO substrate and the dye. The efficiency and *SNR* show the largest values for R6G, followed by SR101 with the lowest value for RhB. The *AEF* is found to be highest for SR101 and again lowest for RhB, with the difference being even more pronounced when one takes into account the lower adsorption ability of the AgGO substrate for SR101.

As seen earlier in table 1 R6G was strongly quenched directly by the GO with an efficiency of ~53%, and the efficiency further increased by ~22% in the presence of the AgGO to ~75%. SR101 exhibited the weakest direct quenching by the GO flakes of ~21%, which could be expected due its lower quantum yield. However, the presence of the Ag NPs in the AgGO substrate induced the largest increase in the efficiency for SR101 resulting in an overall efficiency of ~74% on the AgGO composite. This indicates that emission quenching is a more significant factor in the SERS *SNR* and *AEF* for R6G than for SR101. It also indicates that SR101 is most strongly coupled to the Ag NPs, which would be expected to yield the largest enhancement of the Raman signal. Direct quenching of RhB emission by the GO flakes is 8% lower than for R6G, and while the relative increase of the efficiency for the AgGO composite is similar to that for R6G, the overall efficiency is the lowest of the three dyes, mirroring the lowest *SNR* and *AEF* from the Raman measurements for this dye.

In this study we have shown that the AgGO substrate significantly quenches the fluorescence and enhances the intensity of the Raman peaks for each of the dyes studied at low laser excitation powers. We have demonstrated the application of the composite substrate for Raman detection of high concentrations of dyes ($\sim10^{-3}$-10^{-5} M) whereby under standard Raman or SERS protocol these dyes the strong fluorescence masks the characteristic Raman peaks. This opens up a variety of potential applications for the detection of high concentrations of fluorescent dyes as DNA labels[64] in biological studies and as target analyte molecules in non-biological studies. The adoption of the AgGO SERS

substrate for such studies eliminates the requirement to use dilute concentrations (10^{-7}-10^{-9} M) of dyes in combination with high laser excitation powers to detect these analyte molecules.

4. CONCLUSIONS

The impact of AgGO composite substrates on the fluorescence and Raman signals of dye molecules emitting in the 550 nm to 700 nm range has been examined. Spectral and time-resolved fluorescence measurements reveal the effect on the dye emission of the adsorption of the Ag NPs onto GO flakes, forming AgGO composites. A further reduction of the dye fluorescence lifetime on the AgGO composite compared with the GO flakes indicates even stronger interaction between the dye and the AgGO composite. The interplay between fluorescence and SERS is an important factor in determining the suitability of a substrate for SERS of fluorescent molecules. The emission spectra confirm the strong emission quenching properties of the GO flake with only a small recovery in emission observed after adsorption of the Ag NPs. The dominance of quenching due to the GO component in the composite substrate significantly reduces the fluorescence background in the Raman spectra. The impact of the AgGO substrate on the Raman spectra is quantified by a *SNR* obtained over many measurements to represent an average over the substrate and not a single 'hot-spot' measurement. Large increases in the *SNR* are observed relative to Ag NPs for all dyes, and the high sensitivity of the substrate is further demonstrated by 'hot-spot' detection limits of 10^{-9} M for R6G and 10^{-8} M for RhB and SR101. The *SNR* measurements analysis reveals that R6G benefits most from the substrate with similar improvements in *SNR* observed for RhB and SR101, despite the lower concentration adsorbed for SR101. This is strongly correlated with the TRPL data, showing the largest change in fluorescence lifetime on the AgGO substrate occurs for R6G and SR101. Fluorescence quenching by the GO flakes is a more significant factor in SERS on the AgGO composite for R6G and RhB, with SR101 benefitting most from direct enhancement of the Raman signals.

References

1.   D. L. Jeanmaire and R. P. Van Duyne, *J. Electroanal. Chem.* 84, (**1977**).

2.   M. G. Albrecht and J. A. Creighton, *J. Am. Chem. Soc.* 99, 5215 (**1977**).

3.   M. Fleischmann, P. J. Hendra and A. J. Mcquillan, *Chem. Phys. Lett.* 26, 163 (**1974**).

4.   A. Campion and P. Kambhampati, *Chem. Soc. Rev.* 27, 241 (**1998**).

5.   B. Sharma, R. R. Frontiera, A.-I. Henry, E. Ringe and R. P. Van Duyne, *Materials Today* 15, 16 (**2012**).

6.   M. Fan, G. F. Andrade and A. G. Brolo, *Anal. Chim. Acta* 693, 7 (**2011**).

7.   S. Mehigan, C. A. Smyth and E. M. McCabe, *Nanomat. and Nanotech.* 5, 1 (**2015**).

8.   X. Zou and S. Dong, *J. Phys. Chem. B* 110, 21545 (**2006**).

9.   A. M. Schwartzberg, C. D. Grant, A. Wolcott, C. E. Talley, T. R. Huser, R. Bogomolni and J. Z. Zhang, *J. Phys. Chem. B* 108, 19191 (**2004**).

10.   S. S. Dasary, A. K. Singh, D. Senapati, H. Yu and P. C. Ray, *J. Am. Chem. Soc.* 131, 13806 (**2009**).

11.   J. Zhang, J. Malicka, I. Gryczynski and J. R. Lakowicz, *J. Phys. Chem. B* 109, 7643 (**2005**).

12.   O. Kulakovich, N. Strekal, A. Yaroshevich, S. Maskevich, S. Gaponenko, I. Nabiev, U. Woggon and M. Artemyev, *Nano Lett.* 2, 1449 (**2002**).

13.   V. K. Komarala, Y. P. Rakovich, A. L. Bradley, S. J. Byrne, Y. K. Gun'ko, N. Gaponik and A. Eychmüller, *Appl. Phys. Lett.* 89, 253118 (**2006**).

14.   X. Ling, L. Xie, Y. Fang, H. Xu, H. Zhang, J. Kong, M. S. Dresselhaus, J. Zhang and Z. Liu, *Nano Lett.* 10, 553 (**2010**).

15.   A. Wojcik and P. V. Kamat, *ACS Nano* 4, 6697 (**2010**).

16.   X. Wang, P. Huang, L. Feng, M. He, S. Guo, G. Shen and D. Cui, *RSC Adv.* 2, 3816 (**2012**).

17.   X. Yu, Cai H., W. Zhang, X. Li, N. Pan, Y. Luo, J. G. Hou and X. Wang, *ACS Nano* 5, 952 (**2010**).

18.   Z. Y. Chen, S. Berciaud, C. Nuckolls, T. F. Heinz and L. E. Brus, *ACS Nano* 4, 2964 (**2010**).

19.   A. Yeltik, G. Kucukayan-Dogu, B. Guzelturk, S. Fardindoost, Y. Kelestemur and H. V. Demir, *J. Phys. Chem. C* 117, 25298 (**2013**).

20.   E. Morales-Narváez, B. Pérez-López, L. B. Pires and A. Merkoçi, *Carbon* 50, 2987 (**2012**).

21.   L. Gaudreau, K. J. Tielrooij, G. E. Prawiroatmodjo, J. Osmond, F. J. Garcia de Abajo and F. H. Koppens, *Nano Lett.* 13, 2030 (**2013**).

22.   A. Kasry, A. A. Ardakani, G. S. Tulevski, B. Menges, M. Copel and L. Vyklicky, *J. Phys. Chem. C* 116, 2858 (**2012**).

23.   V. Thangaraj, J. Bussiere, J.-M. Janot, M. Bechelany, M. Jaber, S. Subramanian, P. Miele and S. Balme, *Eur. J. Inorg. Chem.* 2125 (**2016**).

24.   N. C. Berner, S. Winters, C. Backes, C. Yim, K. C. Dumbgen, I. Kaminska, S. Mackowski, A. A. Cafolla, A. Hirsch and G. S. Duesberg, *Nanoscale* 7, 16337 (**2015**).

25.   D. L. Dexter, *J. Chem. Phys.* 21, 836 (**1953**).

26.   E. V. Efremov, F. Ariese and C. Gooijer, *Anal. Chim. Acta* 606, 119 (**2008**).

27.   L. M. Xie, X. Ling, Y. Fang, J. Zhang and Z. F. Liu, *J. Am. Chem. Soc.* 131, 9890 (**2009**).

28.   Z. Zhang, F. Xu, W. Yang, M. Guo, X. Wang, B. Zhang and J. Tang, *Chem. Commun. (Camb)* 47, 6440 (**2011**).

29.   W. Ren, Y. X. Fang and E. K. Wang, *ACS Nano* 5, 6425 (**2011**).

30.   S. Murphy, L. Huang and P. V. Kamat, *J. Phys. Chem. C* 117, 4740 (**2013**).

31.   S. Dutta, C. Ray, S. Sarkar, M. Pradhan, Y. Negishi and T. Pal, *ACS Appl. Mater. Interfaces* 5, 8724 (**2013**).

32.   W. Fan, Y. H. Lee, S. Pedireddy, Q. Zhang, T. Liu and X. Y. Ling, *Nanoscale* 6, 4843 (**2014**).

33.   K. Turcheniuk, R. Boukherroub and S. Szunerits, *J. Mater. Chem. B* 3, 4301 (**2015**).

34.   K. P. Loh, Q. Bao, G. Eda and M. Chhowalla, *Nat. Chem.* 2, 1015 (**2010**).

35.   S. Park and R. S. Ruoff, *Nat. Nanotechnol.* 4, 217 (**2009**).

36.   C. Kavitha, K. Bramhaiah, N. S. John and B. E. Ramachandran, *Chem. Phys. Lett.* 629, 81 (**2015**).

37.   Y. Zhang, S. Liu, L. Wang, X. Qin, J. Tian, W. Lu, G. Chang and X. Sun, *RSC Adv.* 2, 538 (**2012**).

38.   Y. Zhou, X. Cheng, D. Du, J. Yang, N. Zhao, S. Ma, T. Zhong and Y. Lin, *J. Mater. Chem. C* 2, 6850 (**2014**).

39.   J. Huang, L. Zhang, B. Chen, N. Ji, F. Chen, Y. Zhang and Z. Zhang, *Nanoscale* 2, 2733 (**2010**).

40.   G. Ding, S. Xie, Y. Liu, L. Wang and F. Xu, *Appl. Surf. Sci.* 345, 310 (**2015**).

41.   Q. Liu, X. Zhang, G. Wen, Y. Luo, A. Liang and Z. Jiang, *Plasmonics* 10, 285 (**2014**).

42.   X. Liang, T. You, D. Liu, X. Lang, E. Tan, J. Shi, P. Yin and L. Guo, *Phys. Chem. Chem. Phys.* 17, 10176 (**2015**).

43.   X. Gong, J. Tang, Y. Ji, B. Wu, H. Wu and A. Liu, *RSC Adv.* 5, 42653 (**2015**).

44.   K. Zangeneh Kamali, A. Pandikumar, G. Sivaraman, H. N. Lim, S. P. Wren, T. Sun and N. M. Huang, *RSC Adv.* 5, 17809 (**2015**).

45.   A. Saha, S. Palmal and N. R. Jana, *Nanoscale* 4, 6649 (**2012**).

46.   R. Wang, Y. Xu, C. Wang, H. Zhao, R. Wang, X. Liao, L. Chen and G. Chen, *Appl. Surf. Sci.* 349, 805 (**2015**).

47.   H. Hou, P. Wang, J. Zhang, C. Li and Y. Jin, *ACS Appl. Mater. Interfaces* 7, 18038 (**2015**).

48.   M. C. Dalfovo, G. I. Lacconi, M. Moreno, M. C. Yappert, G. U. Sumanasekera, R. C. Salvarezza and F. J. Ibanez, *ACS Appl. Mater. Interfaces* 6, 6384 (**2014**).

49.   S. Sil, N. Kuhar, S. Acharya and S. Umapathy, *Sci. Rep.* 3, 3336 (**2013**).

50.   Y. Liu, Y. Hu and J. Zhang, *J. Phys. Chem. C* 118, 8993 (**2014**).

51.   W. Xu, X. Ling, J. Xiao, M. S. Dresselhaus, J. Kong, H. Xu, Z. Liu and J. Zhang, *Proc. Natl. Acad. Sci. USA* 109, 9281 (**2012**).

52.   L. Fu, D. Zhu and A. Yu, *Spectrochim. Acta. A Mol. Biomol. Spectrosc.* 149, 396 (**2015**).

53.   W. S. Hummers and R. E. Offeman, *J. Am. Chem. Soc.* 80, (**1958**).

54.   C. Xu, X. Wang, J. Zhu, X. Yang and L. Lu, *J. Mater. Chem.* 18, 5625 (**2008**).

55.   A. A. Lazarides and G. C. Schatz, *J. Phys. Chem. B* 104, (**2000**).

56.   H. C. v. d. Hulst, *Light Scattering by Small Particles*. Dover Publication: 1957.

57.   A. Penzkofer and W. Leupacher, *Journal of Luminescence* 37, 61 (**1987**).

58.   P. Anger, P. Bharadwaj and L. Novotny, *Phys. Rev. Lett.* 96, 113002 (**2006**).

59.   E. Dulkeith, A. C. Morteani, T. Niedereichholz, T. A. Klar, J. Feldmann, S. A. Levi, F. C. van Veggel, D. N. Reinhoudt, M. Moller and D. I. Gittins, *Phys. Rev. Lett.* 89, 203002 (**2002**).

60.   S. Kuhn, U. Hakanson, L. Rogobete and V. Sandoghdar, *Phys. Rev. Lett*. 97, 017402 (**2006**).

61.   X. Zhang, C. A. Marocico, M. Lunz, V. A. Gerard, Y. K. Gun'ko, V. Lesnyak, N. Gaponik, A. S. Susha, A. L. Rogach and A. L. Bradley, *ACS Nano* 6, 9283 (**2012**).

62.   M. Ludwig and S. A. Asher, *Appl. Spectrosc.* 42, 1458 (**1988**).

63.   P. Hildebrandt and M. Stockburger, *J. Phys. Chem.* 88, (**1984**).

64.   D. Graham, K. Faulds and W. E. Smith, *Chem. Commun. (Camb)*, 4363 (**2006**).

Captions for figures

Fig. 1.   (a) TEM image of AgGO flake, (b) SEM image of AgGO flake, (c) AFM image of AgGO flake and (d) histogram of distribution of Ag NP diameters on the GO flakes. The scale bars in (a) and (b) are 500 nm.

Fig. 2.   (a) Extinction spectra of GO (red dot), Ag NPs (blue dash) and AgGO (black solid), and (b) extinction (black), absorption (red) and scattering (blue) spectra of AgGO.

Fig. 3.   (a) Extinction spectra of R6G (green), RhB (orange), and SR101 (red) with the black dashed marker representing the Raman laser excitation wavelength. (b) Normalized scattering (black dash) and absorption (blue dot) of AgGO and normalized PL of R6G (green solid), RhB (orange solid) and SR101 (red solid). PL measurements were performed using an excitation wavelength of 405 nm and dye concentrations of 4×10^{-7} M. (c) Histogram representing the percentage of dye adsorbed on the AgGO substrates.

Fig. 4.   (a-c) Fluorescence decay curves for (a) R6G only (blue), on GO (red) and on AgGO (black). (b) RhB only (blue), on GO (red) and on AgGO (black). (c) SR101 only (blue), on GO (red) and on AgGO (black). (d-f) PL spectra for (d) R6G only (blue), on GO (red) and on AgGO (black). (e) RhB only (blue), on GO (red) and on AgGO (black). (f) SR101 only (blue), on GO (red) and on AgGO (black). The dye concentration in each spectrum is 4×10^{-7} M.

Fig. 5.   (a-c) Single Raman spectra of 10^{-4} M (a) R6G on AgGO (black), on Ag NPs (red) and on GO (blue). (b) RhB on AgGO (black), on Ag NPs (red) and on GO (blue). (c) SR101 on AgGO (black), on Ag NPs (red) and on GO (blue). (d-f) Average Raman scattering

spectra for 10^{-4} M of (d) R6G, (e) RhB and (f) SR101. In each panel the spectrum for the dye alone is shown in blue, on the AgGO composite is shown in black and on the Ag NPs is shown in red. The Raman spectra of dye only have a concentration of 10^{-3} M. The red solid [green dash] arrows in (d-f) indicate the peak [noise] positions chosen to calculate the SNR values.

Fig. 6.   SNR distribution on AgGO substrates for (a) R6G, (b) RhB and (c) SR101 and SNR distribution on Ag NP substrates for (d) R6G, (e) RhB and (f) SR101.

Fig. 7.   Concentration dependent Raman scattering spectra for (a) R6G, (b) RhB and (c) SR101.
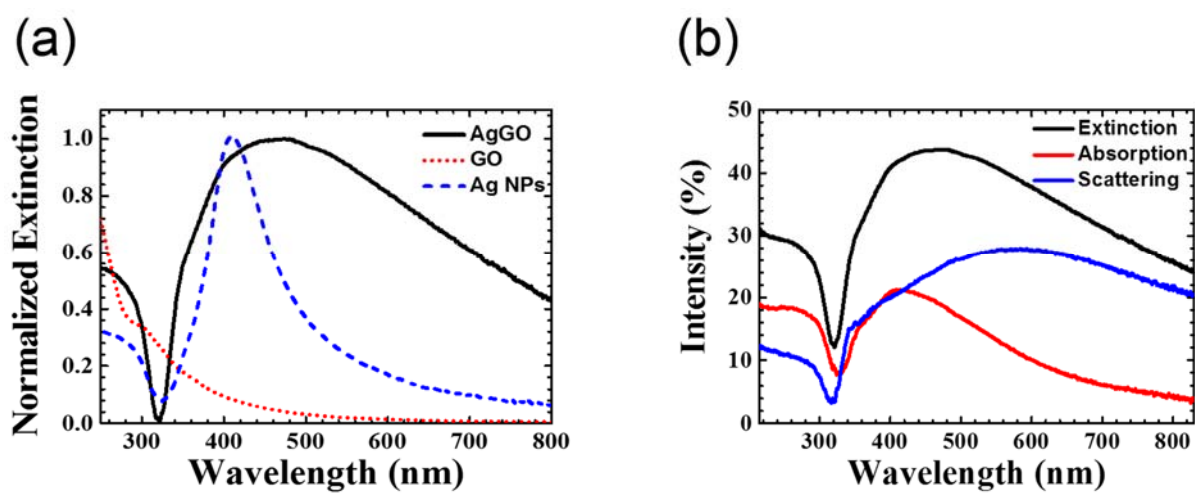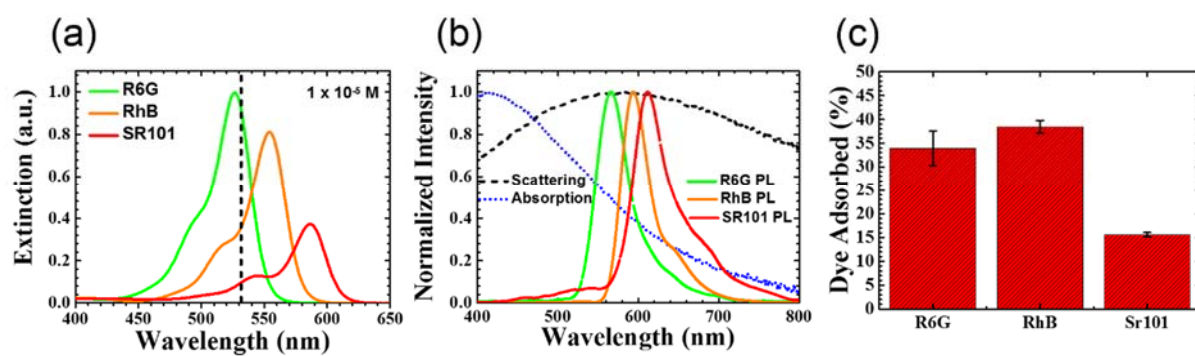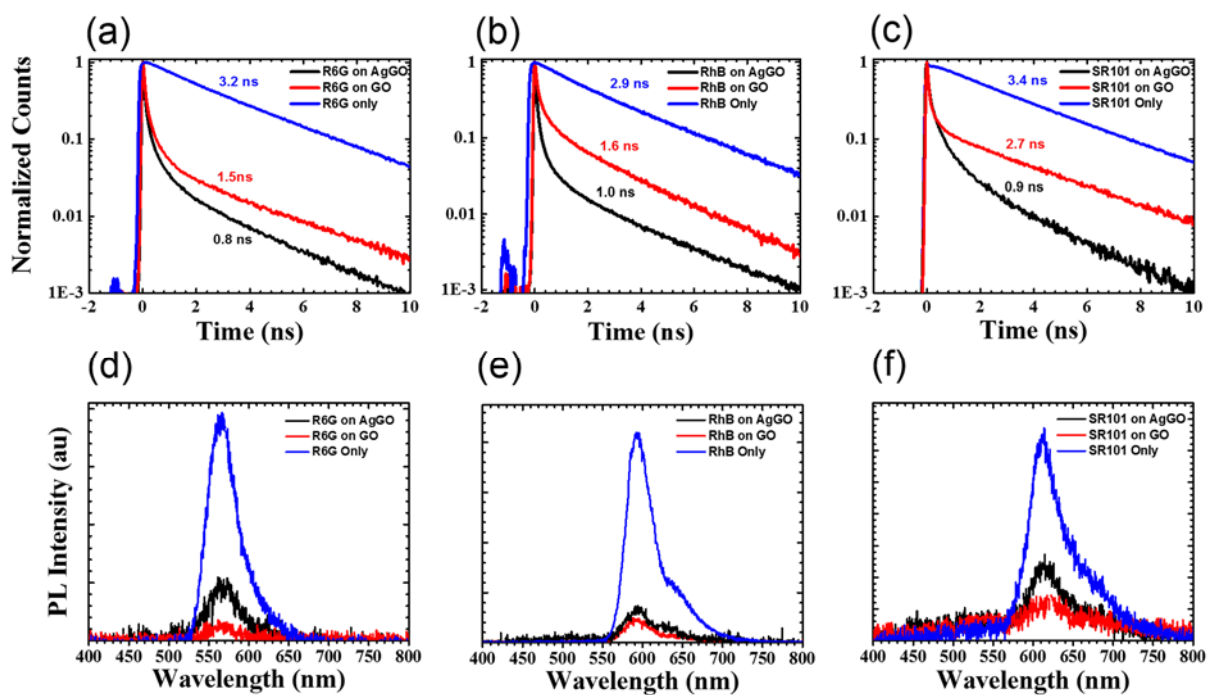
Fig. 1

"Influence of graphene oxide/Ag nanoparticle composites on the fluorescence properties of organic dyes"
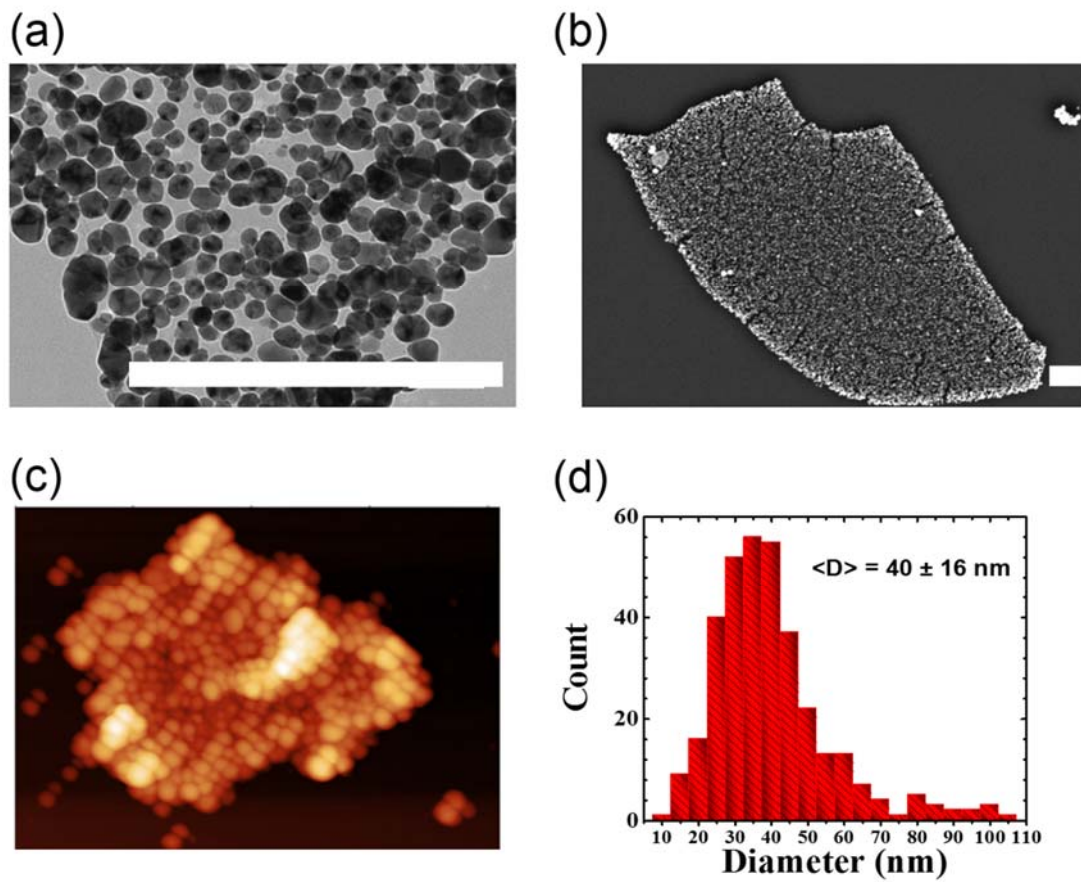
by J. J. Gough *et al.*

Fig. 2

"Influence of graphene oxide/Ag nanoparticle composites on the fluorescence properties of

organic dyes"

by J. J. Gough *et al.*

Fig. 3

"Influence of graphene oxide/Ag nanoparticle composites on the fluorescence properties of organic dyes"

by J. J. Gough *et al.*

Fig. 4

"Influence of graphene oxide/Ag nanoparticle composites on the fluorescence properties of organic dyes"

by J. J. Gough *et al.*

Fig. 5

"Influence of graphene oxide/Ag nanoparticle composites on the fluorescence properties of organic dyes"
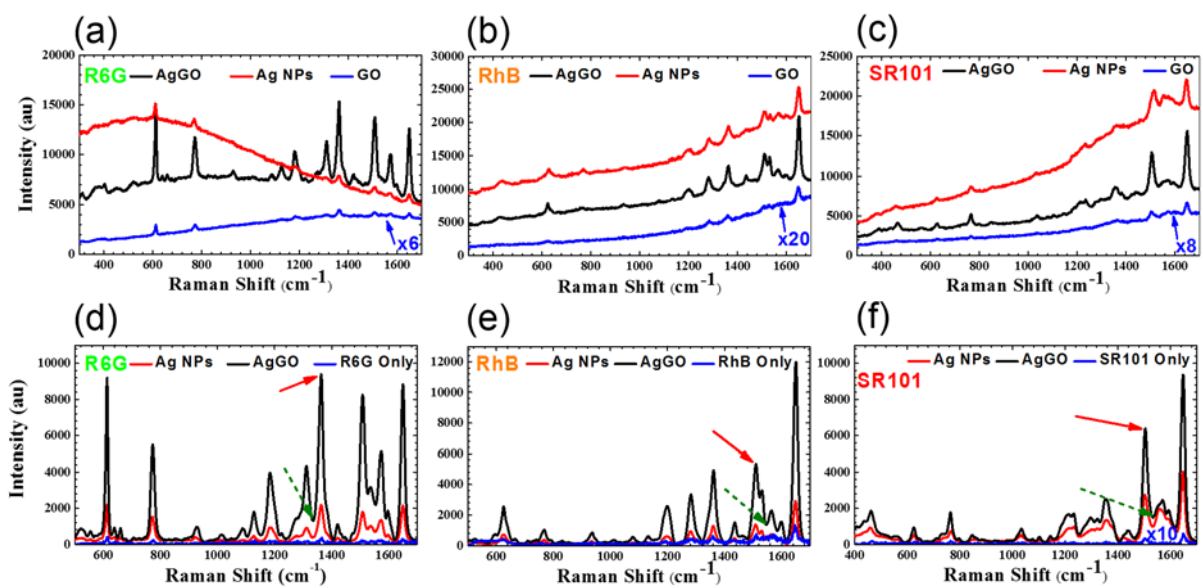
by J. J. Gough *et al.*

Fig. 6

"Influence of graphene oxide/Ag nanoparticle composites on the fluorescence properties of organic dyes"
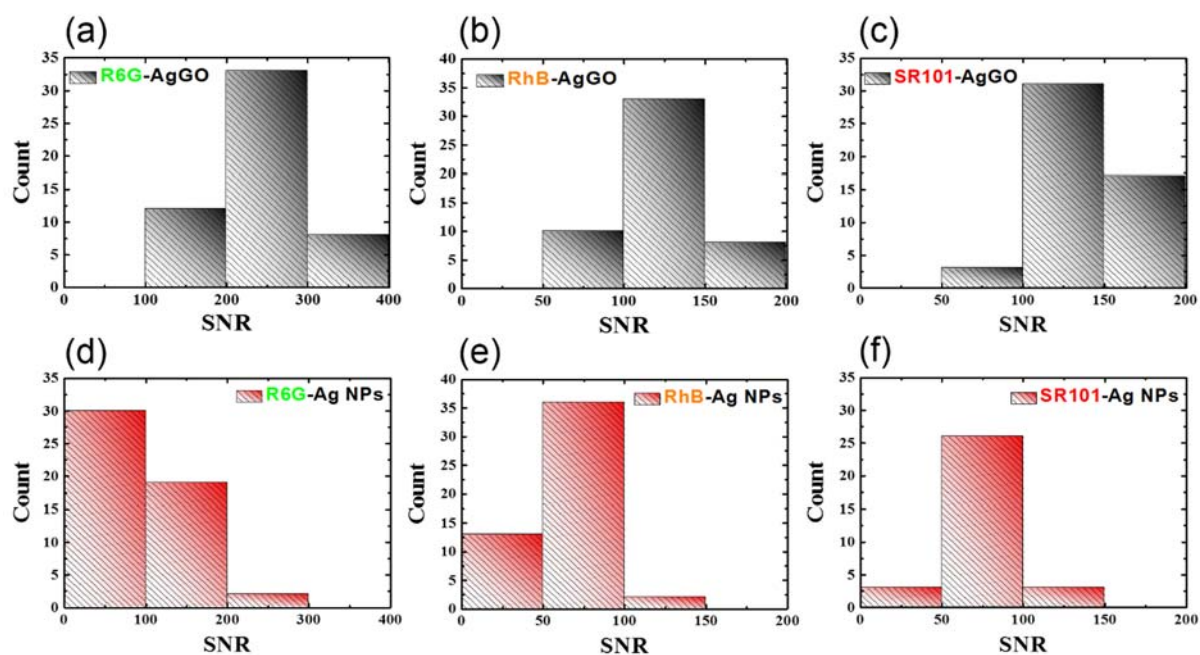
by J. J. Gough *et al.*

Fig. 7

"Influence of graphene oxide/Ag nanoparticle composites on the fluorescence properties of

organic dyes"

by J. J. Gough *et al.*